Supplementary Information

Electrolyte composition dependent Li-ion binding and degradation of organic radical battery material

Davis Thomas Daniel,*[a],[c] Emmanouil Veroutis,[a] P. Philipp M. Schleker ,
[a] Rüdiger-A Eichel,[a],[b] Josef Granwehr [a],[c]

*Corresponding author. Email: **d.daniel@fz-juelich.de**

[a] Institute of Energy Technologies (IET-1), Forschungszentrum Jülich, Jülich 52425, Germany

[b] Institute of Physical Chemistry, RWTH Aachen University, Aachen 52074, Germany

[c] Institute of Technical and Macromolecular Chemistry, RWTH Aachen University, Aachen 52074, Germany

Contents

1 Sample Preparation

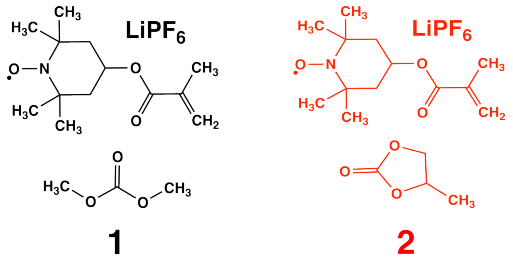

In an argon-filled glove box, TEMPO methacrylate (TMA,4.80 mg, 20 mM, *Sigma Aldrich*) was dissolved in 1 mL of dimethyl carbonate (DMC,*Sigma Aldrich*) and propylene carbonate (PC,*Sigma Aldrich*), each containing 1 M $LiPF_6$, to prepare samples **1** and **2** respectively (see structures above). For EPR investigation, 20 µL of the sample solution was transferred to 2 mm outer diameter (OD) EPR tubes. To study the dependence of TMA degradation on water content, TMA was dried for 1 month at 35°C under argon. The dried TMA powder (4.80 mg, 20 mM) was then dissolved in 1 mL of DMC and PC, each containing 1 M $LiPF_6$, for preparing samples **1**′ and **2**′ respectively. For time resolved NMR experiments, **1** was prepared with a solvent mixture of 90% v/v DMC and 10% v/v deuterated DMC (DMC-d6, 99% atom D, *Sigma Aldrich*). 500 µL of the sample solution was transferred to 5mm OD NMR tubes and 1% v/v of tetramethylsilane (TMS) was added to the sample. For $^{1}H-^{13}C$ HSQC (Heteronuclear Single-Quantum Correlation), $^{1}H-^{1}H$ COSY (Correlation Spectroscopy) and $^{1}H-^{1}H$ NOESY (Nuclear Overhauser Effect Spectroscopy) experiments, sample composition of **1** was the same except for DMC-d6 as the solvent.

2 DFT calculations

2.1 Methods

All DFT calculations were implemented using *ORCA* v.5.0.2. Prior to NMR chemical shift calculations and EPR hyperfine tensor calculations, all paramagnetic species were geometry optimized at UKS/B3LYP/6-31++G(d,p) and all diamagnetic species were optimised at RKS/B3LYP/6-31++G(d,p) level. Resolution of identity approximation was used during the optimisation. DMC solvent was modelled using a conductor-like polarisable continuum model (CPCM) for DMC. NMR chemical shift calculations, EPR g-tensor and EPR hyperfine tensor calculations, were then done using identical functional, basis set and CPCM model for DMC. Chemical shift calculations using identical parameters were also done for TMS as a reference.

The same protocol was used for geometry optimization and hyperfine tensor calculations of a system consisting of TMA bound to $LiPF_6$ with an implicit solvation model. In addition, a geometry optimized structure of TMA with Li-bound to the carbonyl oxygen of the methacrylate branch was also used for ^{7}Li hyperfine tensor calculation.

Nudged elastic band (NEB) calculations were done at UKS/B3LYP/6-31++G(d,p) level using geometry optimised structures of $\mathbf{T}_a$ with HF and $\mathbf{T}_b$ with LiF as reactants and products respectively. CPCM model for DMC and Grimme's D3 dispersion correction[1] was included.

2.2 Conversion of $\mathbf{T}_a$ to $\mathbf{T}_b$

The mean energy pathway of $\mathbf{T}_a$ to $\mathbf{T}_b$ conversion is shown in Figure S1 which indicates a non-spontaneous reaction. $\mathbf{T}_a$ and HF were used as reactants and $\mathbf{T}_b$ and LiF as products.

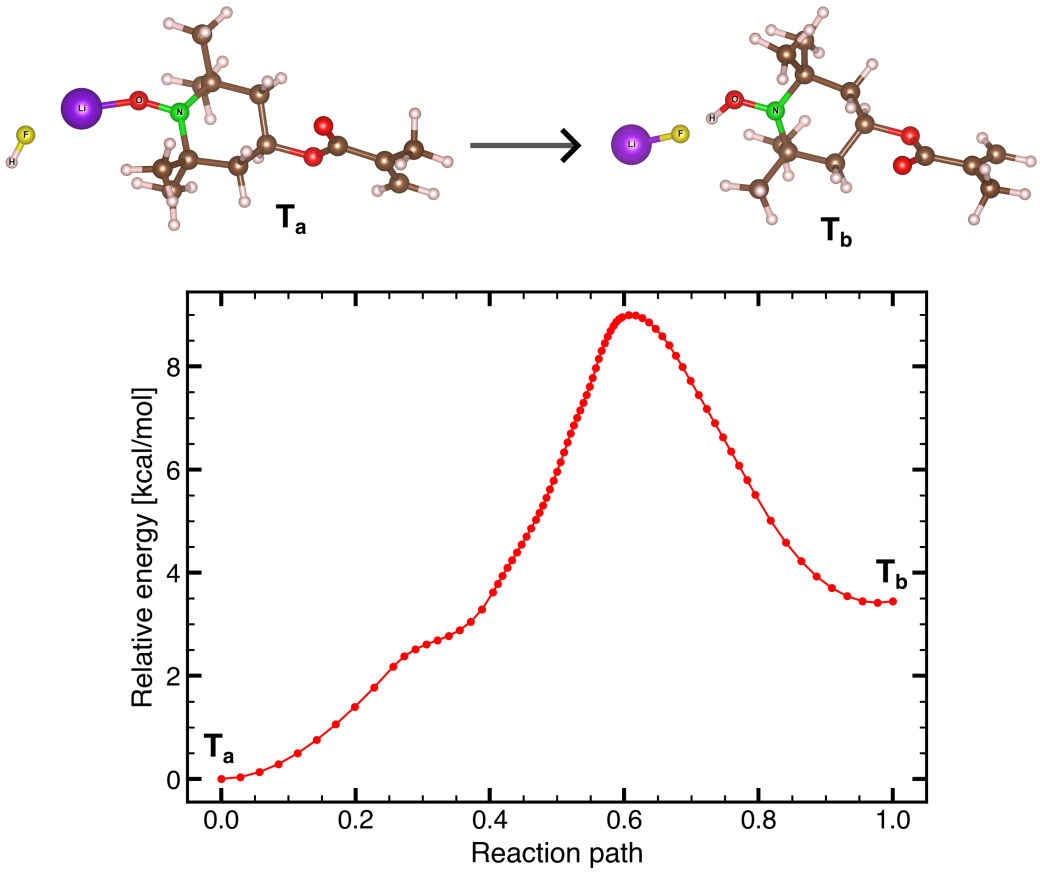

Figure S1: Mean energy pathway for the conversion of $\mathbf{T}_a$ to $\mathbf{T}_b$.

3 EPR spectroscopy

3.1 Experimental

X-Band continous wave (CW) EPR experiments were conducted at 298 K and EPR spectra were obtained as first derivatives of absorption spectra, using a *Bruker* EMX spectrometer operating at 9.65 GHz. A microwave power of 0.3162 mW, modulation amplitude of 0.05 mT and a modulation frequency of 100 kHz was used.

All pulsed EPR experiments were conducted on an X-band *Bruker* ELEXSYS E580 spectrometer

equipped with a *Bruker* EN 4118-X-MD5 pulse ENDOR resonator. The temperature was maintained at 60 K with a helium cryostat (*Oxford Instruments* CF935) and freshly-prepared samples of **1** or **2** were flash frozen using liquid nitrogen before being inserted into the cryostat. A standard two-pulse Hahn echo sequence with $\pi/2$ pulse length of 16 ns, π pulse length of 32 ns and an inter-pulse delay τ of 200 ns was used for acquiring field swept echo detected EPR spectra. For spin echo decay measurements, τ was varied in steps of 8 ns. For T_1 measurements, an inversion recovery sequence ($\pi - T - \pi/2 - \tau - \pi - \tau$ – echo) with a 4-step phase cycle was used. The delay T after inversion was set to an initial value of 400 ns and incremented linearly in steps of 2 µs to obtain a data set with 1024 recovery times. For HYSCORE, the pulse sequence $\pi/2$–τ–$\pi/2$–t_1–π–t_2–$\pi/2$–τ–echo was used with 4–step phase cycling. Values of t_1 and t_2 were set to 96 ns and incremented in steps of 8 ns to obtain a two–dimensional data set of size 128x128. Pulse lengths and τ used for inversion recovery and HYSCORE were the same as for the field–swept echo detected experiment. For obtaining the HYSCORE spectrum, two–dimensional data set was first baseline corrected using a third order polynomial in both dimensions, apodized with a Hamming window function , zero–filled with 1024 points and then a two-dimensional Fourier transform was applied.[2] The final HYSCORE spectrum was symmetrised along the diagonal using methodology reported previously.[3] Data processing and analysis was done using home–written scripts that were run on Python v. 3.9.

3.2 CW EPR of TMA in electrolyte

Figure S2(a) compares the CW EPR spectrum of **1** (black) and **2** (red) and Figure S2(b) shows the EPR spectrum of same concentration of TMA in DMC without $LiPF_6$. The EPR lines are broadened due to spin exchange in the sample without $LiPF_6$.

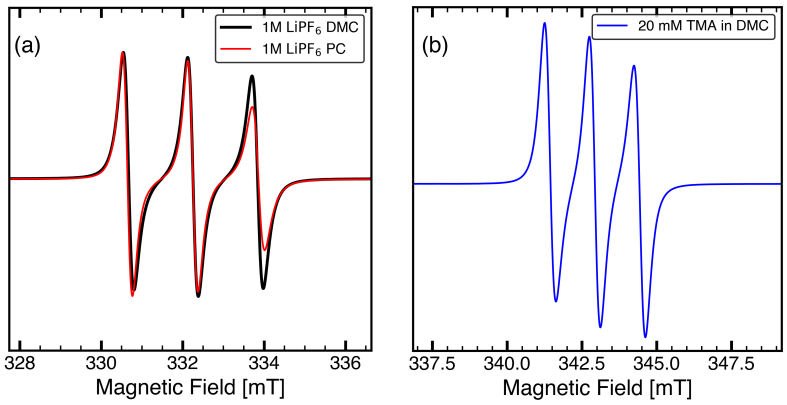

Figure S2: Spin exchange and mobility characteristics of TMA in solution at 298 K. (a) CW EPR of **1** (black) and **2** (red). (b) CW EPR of 20 mM TMA dissolved in DMC in the absence of $LiPF_6$.

3.3 HYSCORE simulation

HYSCORE spectrum of **1** was simulated using a geometry optimised structure of TMA bound to Li. Four DMC solvent molecules were also included in the Li solvation shell based on previous reports.[4] The HYSCORE spectrum was simulated using *saffron* function of EasySpin[5] library with the principal values of tensors obtained from DFT. The simulation parameters are listed in Table S1.

Table S1: DFT-calculated EPR parameters of the structure shown in Figure S3a. The parameters were used for simulating the ^{7}Li cross peaks shown in Figure S3b (red)

Parameter	Value
g-tensor	[2.0094,2.0061,2.0021]
^{7}Li **A**-tensor	[4.0407,4.1927,10.2653]
^{7}Li **Q**-tensor	[-0.1207,-0.3792,0.5000]*10^{-3}

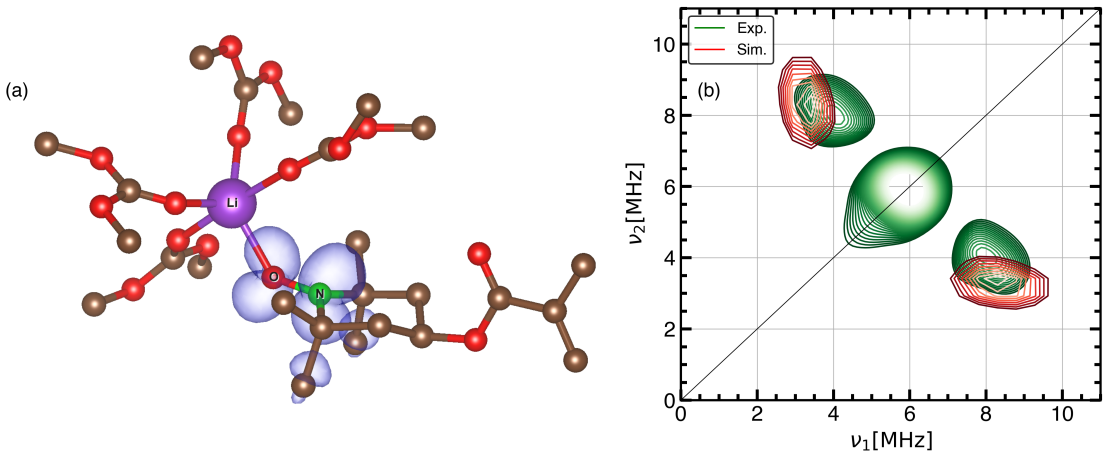

Figure S3: (a) Geometry optimised structure of TMA bound to DMC-solvated Li ion. Distance between Li and the oxygen atom of the nitroxide moiety of TMA was found to be 0.21 nm. Positive spin density is shown with the blue isosurface, carbon atoms are colored brown and oxygen atoms are colored red. Protons are omitted from the depiction for clarity.(b) Comparison of ^{7}Li cross peaks in experimental (green) and simulated (red) HYSCORE spectrum of **1**.

DFT calculations of a separate system containing TMA and $LiPF_6$ with only an implicit model for DMC resulted in similar principal values of [3.8559,4.3047,12.0030] for the ^{7}Li hyperfine tensor. Hyperfine interaction between ^{31}P, ^{19}F nuclear spins and the electron spin was found to be negligible. In contrast to Li binding at the oxygen atom of the N−O moiety of TMA, for Li ion binding to the carbonyl group of the methacrylate branch of TMA, DFT-predicted hyperfine coupling was much smaller in magnitude with principal values of [-0.1426, -0.1455, 0.3006] for the ^{7}Li hyperfine tensor (a_{iso} = 0.0042 MHz).

4 NMR spectroscopy

4.1 Experimental

Time resolved NMR-spectroscopy to study the evolution of ^{1}H NMR spectrum of **1** was done on Bruker Avance III HD spectrometer operating at 400 MHz (^{1}H) equipped with a 5 mm BBO-H Z Gradient probe.^{1}H chemical shifts (δ) were referred to an internal TMS reference at 0 ppm. ^{1}H NMR spectra in time steps of 5 minutes were acquired with an acquisition time 1.28 s, spectral width of 6410.2 Hz, 90° pulse length of 15 µs and a relaxation delay of 2 s. Time resolved NMR spectra were recorded with solvent suppression using an excitation sculpting pulse sequence.[6] For processing, the raw data matrix of size 16384 x 512 was zero filled to 32768 x 512 prior to the application of an exponential window function along the F2 axes, Fourier transformation, phase correction and baseline correction.

2D ^{1}H COSY, ^{1}H NOESY, ^{13}C HSQC experiments were performed by utilizing the standard Bruker pulse sequences *cosygpmfqf*, *noesygpphzs2*, *hsqcedetgpsisp2.4*. For COSY a double quantum filter was utilized in order to minimize diagonal contributions from non-coupled spins,[7] whereas in NOESY a zero quantum suppression was employed in order to minimize COSY-type artifacts arising from *J*-coupled spins.[8]. In HSQC, multiplicity selection was utilized where the signals of CH, CH_3 groups have positive phase, whereas those of CH_2 have negative. Relevant parameters which were used for the 2D experiments are summarized in Table S2. For processing, sine-bell window functions were used along the F1 and F2 axes prior to Fourier transformation, phasing and baseline correction.

Table S2: Parameters used for 2D NMR experiments. D8 is the mixing time used in NOESY and cnst2 is the constant to account for $^{1}J_{\mathrm{H-C}}$ evolution during INEPT.

Exp.	D1 [s]	NS	SW2	SW1	TD2/SI2	TD1/SI1	D8 [s]	cnst2 [Hz]
COSY	2	8	13	13	2048/2048	256/2048	-	-
NOESY	3	16	12	12	2048/2048	256/2048	0.3	-
HSQC	2	8	16	200	2048/2048	256/1024	-	145

For identification of electrolyte degradation products, NMR experiments were conducted on a spectrometer operating at 600 MHz (^{1}H) equipped with a 5 mm BBO-H/F diffusion probe. ^{19}F NMR spectrum of a degraded sample was acquired with an acquisition time 1.44 s, spectral width of 45454.5 Hz, 90° pulse length of 19 µs and a relaxation delay of 2 s. Proton decoupled ^{31}P NMR spectrum of a degraded sample was acquired with an acquisition time 1.34 s, spectral width of 49019.6 Hz, 90° pulse length of 18 µs and a relaxation delay of 2 s. ^{19}F and ^{31}P signals of the degradation products were referred to ^{19}F and ^{31}P signals of $LiPF_6$ at -72.4 ppm and -146.1 ppm.[9] Processing of ^{19}F and ^{31}P data was done in the same manner as the ^{1}H NMR data. NMR data processing and analysis was done using Nmrglue[10] v. 0.9 and home-written python scripts which were run on Python 3.9.

4.2 Electrolyte mediated radical degradation

^{19}F and ^{31}P NMR spectroscopy of **1** after complete radical degradation indicate multiple fluorophos-

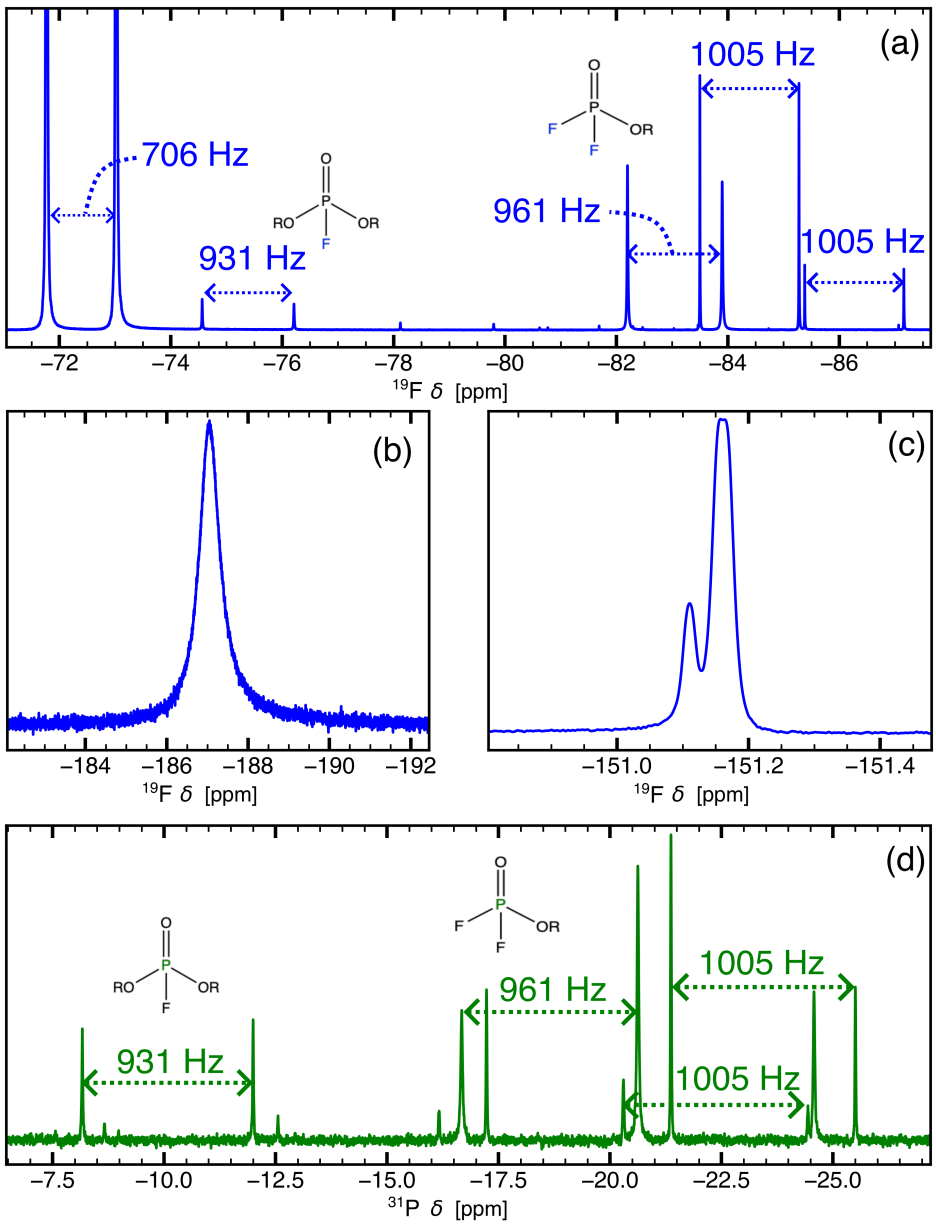

Figure S4: Degradation products of $LiPF_6$ electrolyte investigated using NMR techniques for **1**. (a) ^{19}F NMR spectrum showing the presence of fluorophosphate degradation products. (b)HF species formed as a result of electrolyte degradation. (c)BF_4^- species formed as a result of HF reaction with the NMR glass tube. (d) ^{31}P NMR spectrum showing the presence of fluorophosphate degradation products.

phate degradation products (see Figure S4). The ^{19}F spectrum shows doublets split by the one-bond J-coupling between ^{19}F and ^{31}P nuclear spin (see Figure S4a). Peaks from ^{19}F in $LiPF_6$ are centered at -72.4 ppm and split by 706 Hz. Peaks from the fluorophosphates are centered at -75.31 ppm, -82.97 ppm, -84.31 ppm and -86.19 ppm. The peaks are coupled to corresponding peaks in the ^{31}P spectrum as indicated by same J–coupling in Figure S4(d). Two types of fluorophosphates can be identified, first of the type OPF_2OR which exhibits doublets in the ^{19}F and triplets in ^{31}P. The second type with the

structural formula $OPF(OR)_2$ exhibits doublets in both ^{19}F and ^{31}P spectra. Possible R groups in case of DMC as a solvent are H, CH_3 and Li.[9] The ^{19}F doublets and ^{31}P triplets with a one-bond J coupling of 1005 Hz can be assigned to OPF_2OCH_3, in agreement with previous reports[9, 11] on decomposition products observed for $LiPF_6$ in DMC. The species of type $OPF(OR)_2$ with one-bond J coupling of 931 MHz has been previously assigned to $OPF(OH)_2$.[11, 12] Another OPF_2OR type species is present with a one-bond J coupling of 961 MHz, and is assigned to OPF_2OH.[13] . Presence of HF is indicated by the broad singlet peak at -187.5 ppm (see Figure S4(b)) and the presence of BF_4^- species at -151.1 ppm (see Figure S4(c)).[13] The BF_4^- is formed as a reaction of HF with the borate glass of the NMR tube[13, 14] and results in two singlets corresponding to the ^{11}B and ^{10}B nuclear spins. Presence of boron species was also confirmed by ^{11}B NMR spectroscopy (see Figure S5).

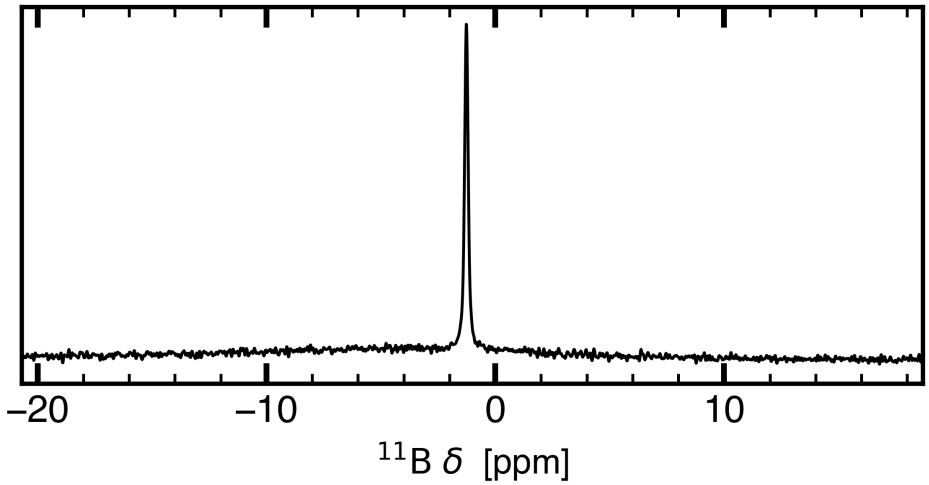

Figure S5: ^{11}B NMR spectrum of **1** after complete radical degradation. Sample : 20 mM TMA in DMC-d6 containing 1 M $LiPF_6$

To identify species related to electrolyte degradation already present in the electrolyte prior to the addition of TMA, ^1H NMR measurements of 1 M $LiPF_6$ in DMC and PC without TMA was done. Hereafter, these samples are referred to as neat DMC or neat PC electrolyte. ^1H NMR spectrum of neat DMC and PC electrolyte is compared in Figure S6. In case of neat DMC electrolyte, NMR resonance corresponding to water was identified at 4.47 ppm (see inset of Figure S6) with an integral of 0.007% relative to the DMC resonance. In case of neat PC electrolyte, water content was not quantified due to the overlap of peaks. A comparison of ^1H NMR spectrum of **1** and the neat DMC electrolyte allows for identifying ^1H peaks which correspond to species that originate from the electrolyte. The neat DMC electrolyte shows two weak ^1H peaks at 4.47 ppm and 3.34 ppm which are assigned to trace water and methanol (CH_3OH) respectively (see inset of Figure S6).[15] Similar to the neat DMC electrolyte, weak ^1H peaks are observed at 4.47 ppm and 3.34 ppm in the ^1H NMR spectrum of **1** (see Figure S8(c) and (d)). In addition, a doublet is observed at 4.22 ppm with four-bond J_{H-P} of 12 Hz which is assigned to OPF_2OCH_3 (see Figure S8(d)).[13, 14] The chemical shifts and J–couplings of all assigned species related to electrolyte degradation are summarised in Table S4. The time evolution of the weak signals at 3.34 ppm, 4.22 ppm and 4.47 ppm during radical degradation in **1** is shown in Figure S7.

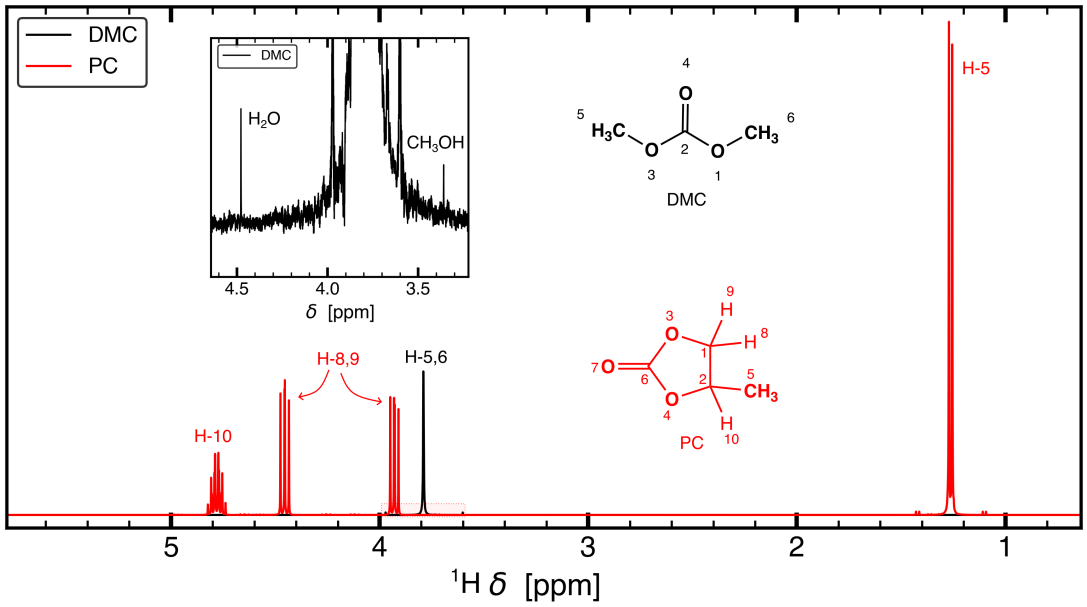

Figure S6: ^{1}H NMR spectrum of 1M $LiPF_6$ in DMC (black) and PC (red) without TMA. Inset shows the chemical shift region of the NMR peak corresponding to water and methanol in DMC.

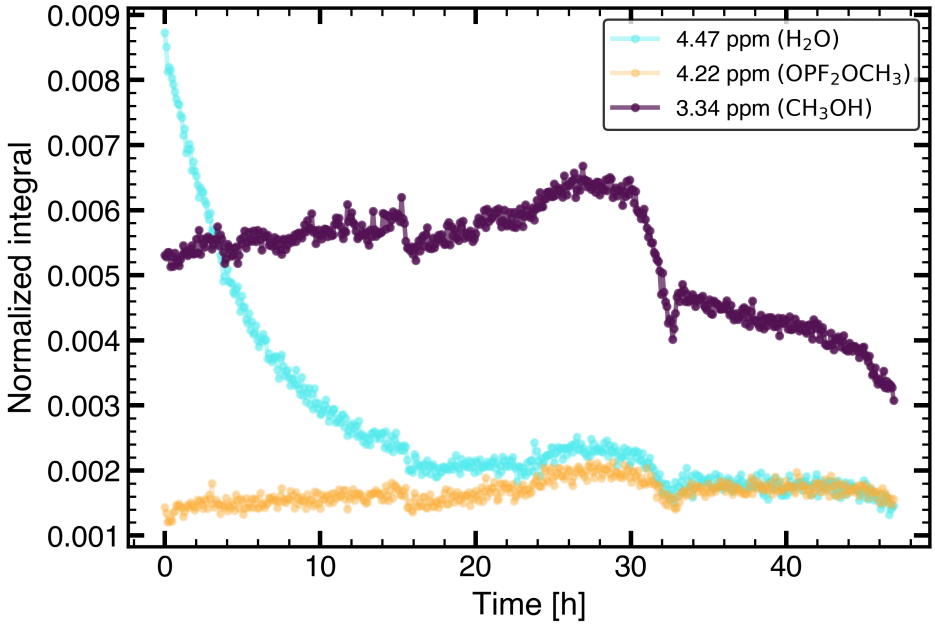

Figure S7: Time evolution of integral of ^{1}H peaks corresponding to water, OPF_2OCH_3 and OPF_2OH in case of TMA degradation in **1**. The integrals were normalised to the integral of the NMR resonance at 1.67 ppm (t = 48 hours).

Both CH_3OH and OPF_2OCH_3 show a slight increase until $t \approx 30$ hours followed by a rapid decrease while water is consumed exponentially until 17 hours. The trend of variation in amounts of these species with time indicates their participation in electrolyte degradation and consequently radical degradation. For $t < 17$ hours, water is consumed to hydrolyse DMC and $LiPF_6$ to produce CH_3OH and HF respec-

tively through linear electrolyte degradation pathways (see Figure 4 in the main text). At $t \approx$30 hours, CH_3OH initiates the cyclic auto-catalytic mechanism involving POF_3 and OPF_2OCH_3 (see Figure 4 in the main text). Simultaneously, formation of $\mathbf{T}_c$ and $\mathbf{T}_e$ takes place through acidic disproportionation due to HF. Note that OPF_2OCH_3 may also be deposited separately through the linear formation pathway (pathway **D** in Figure 4 of the main text) as indicated by the slow increase until 30 hours.

4.3 Assignment of NMR resonance peaks of $\mathbf{T_c}$ and $\mathbf{T_e}$

For further assignment of NMR resonance peaks to the structures, ^{13}C–DEPT135 , ^{13}C HSQC , COSY and ^{1}H$-^1$H NOESY experiments were conducted using a completely degraded sample of **1**. ^{13}C–DEPT135 NMR and HSQC was used to find the hybridisation of carbon nuclei to which the protons are bonded to. In a DEPT135, CH_3 and CH groups appear with a positive phase while CH_2 groups appear with a negative phase. In a ^{13}C HSQC spectrum (see Figure S11), correlation peaks for ^{1}H$-^{13}$C single bond correlations are observed. In ^{1}H$-^1$H COSY spectrum, correlation peaks appear from J-coupled protons which are usually separated by less than four bonds (see Figure S9) while in the case of NOESY, correlation peaks corresponding to protons which are spatially close (up to about 0.5 nm) to each other are present.

The set of doublets in the downfield region (see Figure S8(e)) aid in identifying the peaks that correspond to $\mathbf{T}_e$ and $\mathbf{T}_c$. From the NOESY spectrum, it was found that the O$-$H group of $\mathbf{T}_e$ is correlated to CH_3 protons at 1.67 ppm and CH_2 protons at 2.49 ppm (see Figure S10), indicating that these protons are in spatial proximity. By inspecting the COSY spectrum, peaks of $\mathbf{T}_e$ can therefore be identified (see Figure S9). For comparable protons, NMR signals of $\mathbf{T}_e$ appear more upfield than $\mathbf{T}_c$. As shown in Table 1 in the main text, DFT-derived chemical shifts of $\mathbf{T}_e$ and $\mathbf{T}_c$ agree with this trend. Peaks at $t = 0$ can be classified into two paramagnetic species, Li-bound TMA ($\mathbf{T_a}$) and Li-free TMA ($\mathbf{T'_a}$), as discerned from the HYSCORE experiment using **1**. Peaks shown in Figure S8(a) ranging from 1.6 ppm to 2.1 ppm consists of only methyl protons. (see also Figure S11) The peak in this region at 1.67 ppm for t = 0 arises from the methyl protons 8,9,10 and 11 of $\mathbf{T_a}$ or $\mathbf{T'_a}$. At t = 0, this region also consists of two additional methyl groups (marked by the number 17 at t = 48 hours) at 1.93 ppm and 2.00 ppm. Apart from the already assigned methyl groups, the only other methyl group (DMC methyl groups show peaks at 3.79 ppm) in the $\mathbf{T}'_a$ structure is present in the methacrylate branch (protons marked 17) and the peak at 1.92 ppm can be assigned accordingly to this CH_3 group (C-17 in $\mathbf{T}_e$). Moreover, COSY spectrum indicates that these peaks are coupled to H22 and H23 peaks (see H 22,23–H 17 in Figure S9) assigned later in this section. The four methyl groups flanking the N$-$O moiety in case of $\mathbf{T}_c$ (centred at 1.88 ppm and 1.94 ppm) appear later at $t \approx$ 30 hours and are found to be inequivalent.

The regions shown in Figure S8(b) and (c) consist of only CH_2 groups (see also Figure S11). In the region shown in Figure S8(c) peaks at 2.97 ppm and 3.20 ppm are resolved only at $t \approx$ 30 hours and thus originate from $\mathbf{T}_c$. The peaks show a doublet of doublet splitting pattern, and are assigned to protons attached to C2 and C4 carbons of the $\mathbf{T}_c$ structure. The assignment is further supported by the observation of COSY cross peaks for these protons (see H 19,21–H 18,20 (green) in Figure S9). The doublet

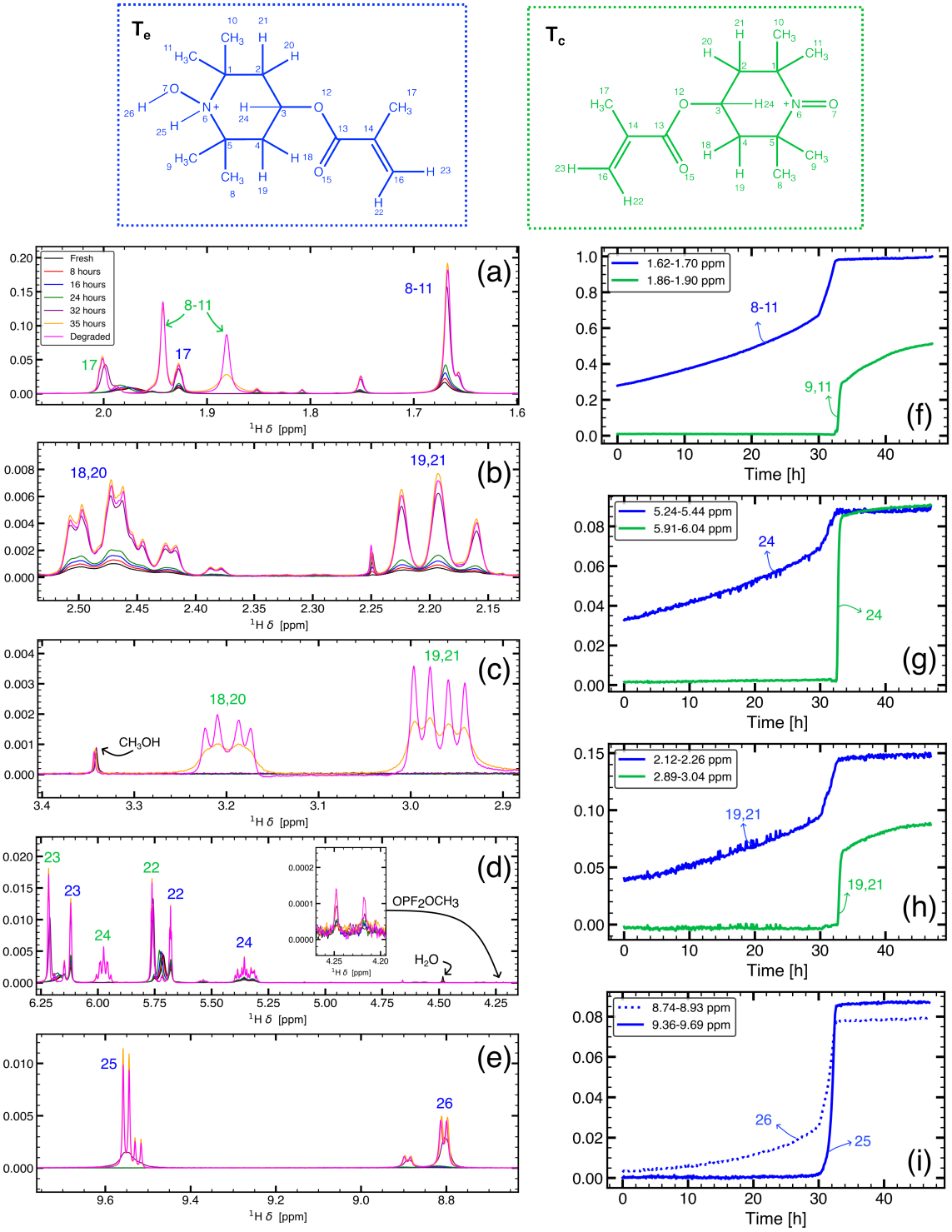

Figure S8: Assignment of NMR resonance peaks to structures of $\mathbf{T_c}$ and $\mathbf{T_e}$.The structures of $\mathbf{T_c}$ and $\mathbf{T_e}$ are shown at the top with numbered protons. The full spectrum is divided into smaller spectral regions shown as a function of time in (a)-(e). Contributions from $\mathbf{T_e}$ and $\mathbf{T_c}$ are annotated with numbers coloured blue and green respectively. Normalised NMR integrals as a function of time for specific protons of $\mathbf{T_c}$ (green) and $\mathbf{T_e}$ (blue) are compared in (f)-(i). The integrals were normalised to the integral of the NMR resonance at 1.67 ppm (t = 48 hours)

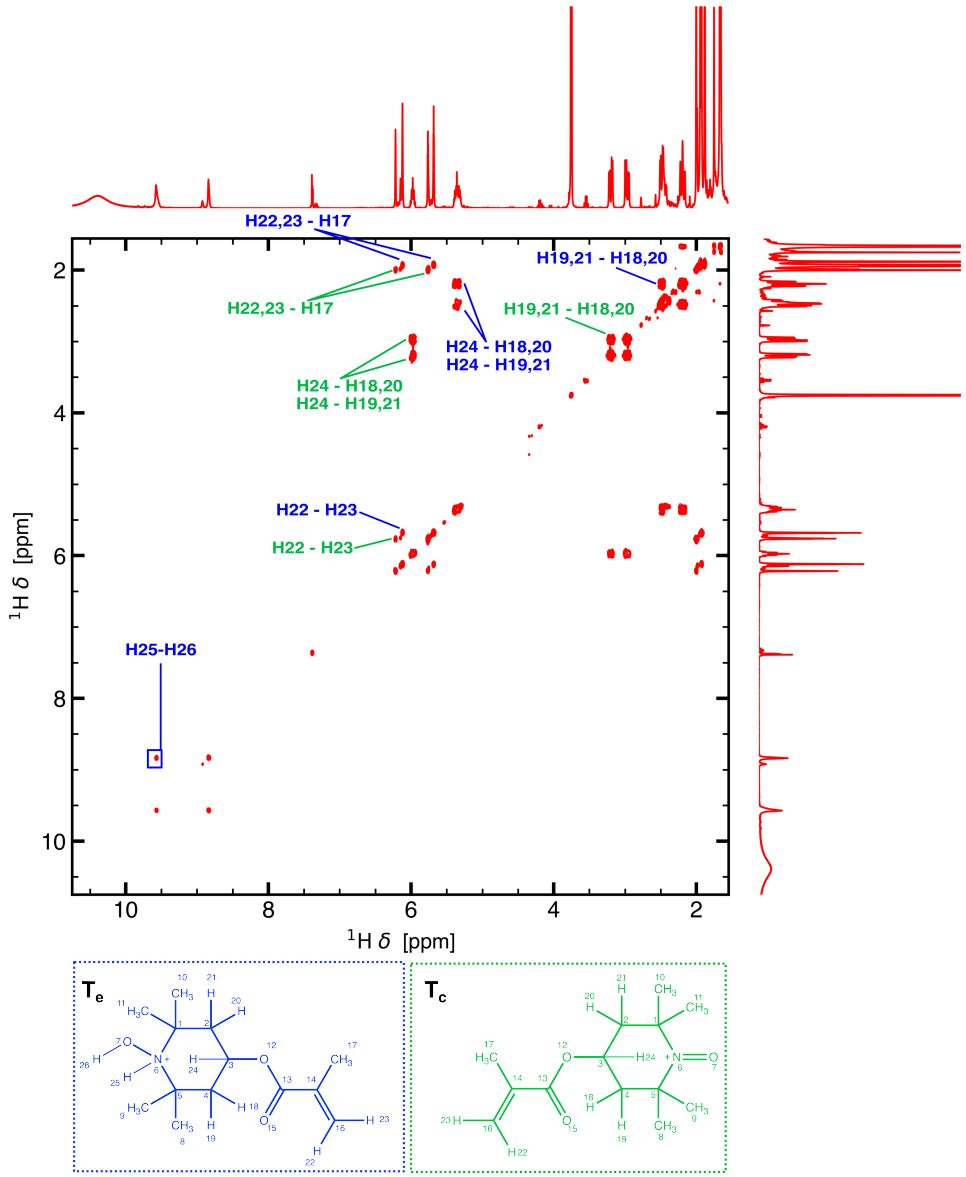

Figure S9: ^{1}H – ^{1}H COSY correlation plot after complete radical degradation. The structures of $\mathbf{T_c}$ and $\mathbf{T_e}$ are shown at the bottom with numbered protons and carbon atoms. Sample : 20 mM TMA in DMC-d6 containing 1 M $LiPF_6$

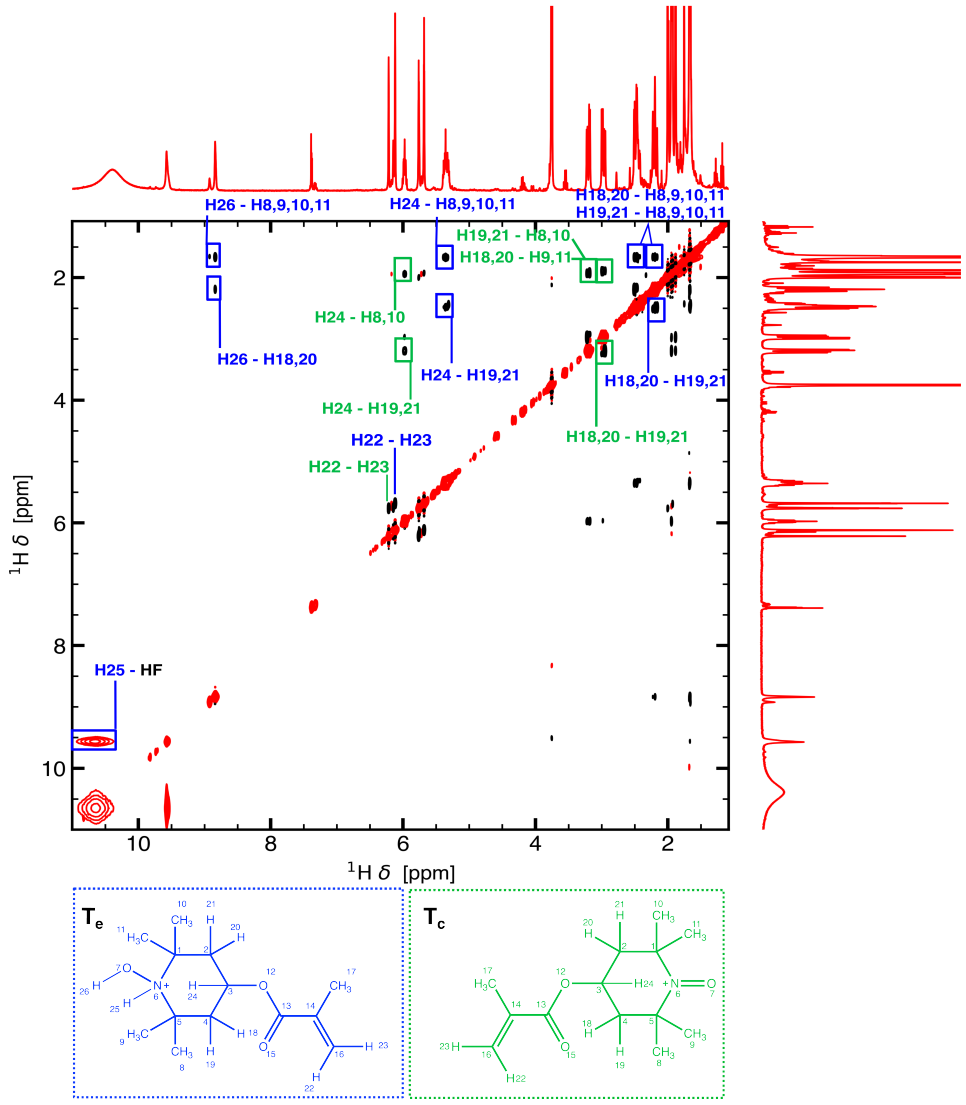

Figure S10: ^{1}H – ^{1}H NOESY correlation plot after complete radical degradation. The structures of $\mathbf{T_c}$ and $\mathbf{T_e}$ are shown at the bottom with numbered protons and carbon atoms. Cross peaks which are anti-phase with respect to the diagonal (black) indicate NOEs whereas in-phase cross peaks (red) indicate exchange (see H25–HF). Sample : 20 mM TMA in DMC-d6 containing 1 M $LiPF_6$

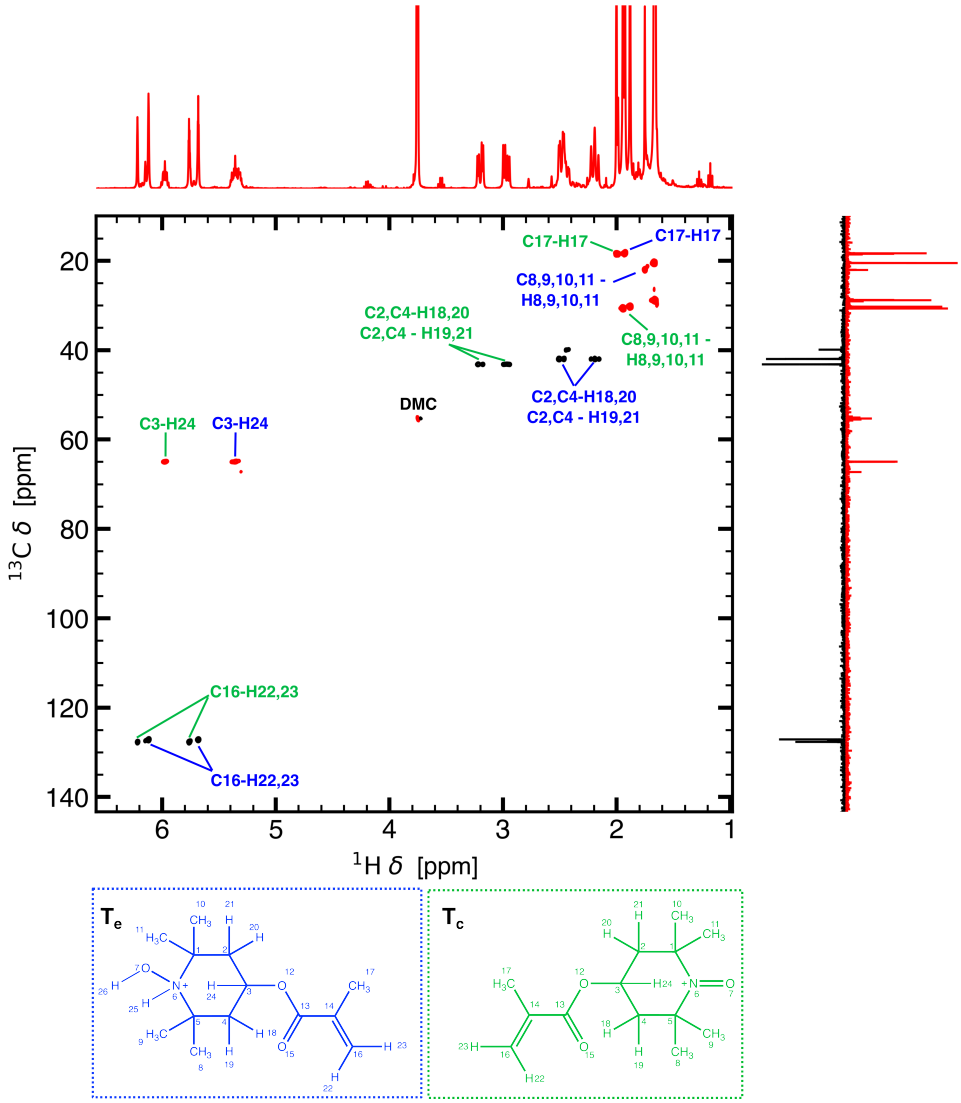

Figure S11: $^{1}H-{}^{13}C$ HSQC correlation plot after complete radical degradation. The structures of $\mathbf{T_c}$ and $\mathbf{T_e}$ are shown at the bottom with numbered protons and carbon atoms. Sample : 20 mM TMA in DMC-d6 containing 1 M $LiPF_6$

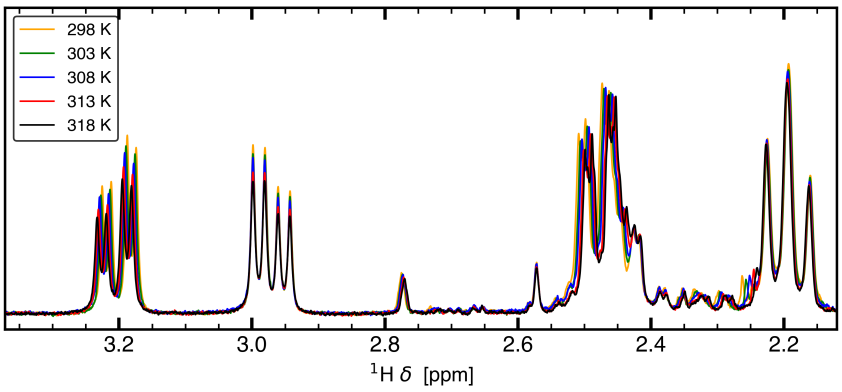

Figure S12: ^{1}H NMR spectrum of **1** as a function of temperature for CH_2 protons (H18,19,20,21) of $\mathbf{T}_c$ and $\mathbf{T}_e$

of doublets splitting also indicates that the geminal protons attached to C2 (H20 and H21) and C4 (H18 and H19) are inequivalent. Such an inequivalence could arise from the tendency of the methacrylate branch to occupy an equatorial position on the six–membered ring. Furthermore, the NOESY spectrum indicates that H24 is correlated to only one set of the geminal protons (see H24–H19,21 in Figure S10). Consequently, the axial and equatorial protons of C2 and C4 carbons experience different environments. Corresponding signals for $\mathbf{T}_e$ centred at 2.19 ppm and 2.49 ppm show similar splitting patterns, but are not clearly resolved due to overlap from other minor signals, possibly from $\mathbf{T}_d$ species which has not undergone the second protonation at N atom to form $\mathbf{T}_e$. Similar to $\mathbf{T}_c$, cross peaks in the COSY spectrum corresponding H18, H19, H20 and H21 are also observed in case of $\mathbf{T}_e$ (see H 19,21–H 18,20 (blue) in Figure S9). Difference in environments between the axial and equatorial CH_2 protons is also evident when the temperature dependence of the chemical shifts is considered (see Figure S12). For both $\mathbf{T}_c$ and $\mathbf{T}_e$, H – 19,21 show no change in resonance peak positions in the temperature range of 298 K to 318 K, while H – 18,20 shift downfield by 0.01 ppm in both cases at 318 K.

The ethylene protons from the methacrylate branch, H22 and H23, appear in the 5.6 ppm to 6.3 ppm region and are also resolved as broad peaks at t = 0 (see Figure S8d). Peaks centred at 5.67 ppm and 6.12 ppm are correlated (see H22–H23, (blue) in Figure S9) and can be assigned to H22,H23 of $\mathbf{T}_e$. Similarly, peaks centred at 5.77 ppm and 6.22 ppm are correlated (see H22–H23, (green) in Figure S9) and can be assigned to H22,23 of $\mathbf{T}_c$.

In both $\mathbf{T}_c$ and $\mathbf{T}_e$, H24 has only the CH_2 protons as nearest neighbors with a three-bond ^{1}H – ^{1}H coupling, evident from the COSY correlation peaks (see H24–H18,19 in Figure S9). As the geminal protons on C2 and C4 are inequivalent, a triplet of triplets splitting pattern is observed for H24 and can therefore be assigned to the peak centered at 5.35 ppm in case of $\mathbf{T}_e$ and 5.97 ppm in case of $\mathbf{T}_c$. NMR shifts and couplings for relevant species in this work is summarized in section 4.4, Table S4 and Table S3. The full ^{1}H and ^{13}C NMR spectrum of **1** after radical degradation in 1M $LiPF_6$/DMC-d6 is shown in Figure S14.

4.4 NMR data

$\mathbf{T}_e$ (Time resolved NMR experiment, t = 48 hours) : ^{1}H NMR (400 MHz, DMC, 298 K, TMS, ppm): δ = 1.67 (s, 12H), 1.93 (s, 3H), 2.19 (dd, *J* = 14.0, 11.5 Hz, 2H), 2.49 (dd, *J* = 14.0, 4.1 Hz, 2H), 5.36 (tt, *J* = 11.7,4.1 Hz, 1H), 5.68 (t, *J* = 1.5 Hz, 1H), 6.12 (dd, *J* = 1.5,0.9 Hz, 1H), 8.76 (d,*J* = 5.6 Hz), 9.55 (d,*J* = 5.6 Hz). ^{13}C{^{1}H} NMR (DMC, 100 MHz) : δ = 18.3(CH_3), 20.5(CH_3), 28.8(CH_3), 42.0(CH_2), 64.95(CH), 127.1(CH_2)

$\mathbf{T}_c$ (Time resolved NMR experiment, t = 48 hours) : ^{1}H NMR (400 MHz, DMC, 298 K, TMS, ppm): δ = 1.88 (s, 6H), 1.94 (s, 6H), 2.00 (s, 3H), 2.97 (dd, *J* = 15.0, 7.2 Hz, 2H), 3.20 (dd, *J* = 15.0, 5.4 Hz, 2H), 5.97 (tt, *J* = 7.1,5.4 Hz, 1H), 5.76 (t, *J* = 1.5 Hz, 1H), 6.22 (dd, *J* = 1.5,0.95 Hz, 1H). ^{13}C{^{1}H} NMR (DMC, 100 MHz) : δ = 18.5(CH_3), 30.3(CH_3), 30.7(CH_3), 43.2(CH_2), 64.97(CH), 127.7(CH_2)

Electrolyte (1 M $LiPF_6$ after complete radical degradation) : ^{19}F NMR (600 MHz, DMC-d6, 298 K, $LiPF_6$, ppm): δ = -72.40 (d, *J* = 706 Hz), -75.31 (d, *J* = 931 Hz), -82.97 (d, *J* = 961 Hz), -84.31 (d, *J* = 1005 Hz), -86.19 (d, *J* = 1005 Hz). ^{31}P NMR (600 MHz, DMC-d6, 298 K, $LiPF_6$, ppm) : -10.09 (d, *J* = 931 Hz), -20.63 (t, *J* = 961 Hz), -21.37 (t, *J* = 1005 Hz), -20.31 (d, *J* = 1005 Hz), -146.10 (sextet, *J* = 706 Hz).

Table S3: Spin-spin couplings for $\mathbf{T}_c$ and $\mathbf{T}_e$ species in **1**

Atomic index	$J^{\text{Exp.}}_{\mathbf{T_c}}$ [Hz]	$J^{\text{Exp.}}_{\mathbf{T_e}}$ [Hz]
H-18,20	15.0, 5.4 (dd)	13.9, 4.1 (dd)
H-19,21	15.0, 7.2 (dd)	14.0, 11.5 (dd)
H-22	1.5 (t)	1.5 (t)
H-23	1.6, 0.95 (dd)	1.6, 0.9 (dd)
H-24	7.1, 5.4 (tt)	11.7, 4.1 (tt)
H-25	-	5.6 (d)
H-26	-	5.6 (d)

Table S4: ^{19}F, ^{31}P and ^{1}H chemical shifts of species related to electrolyte degradation present in **1**

Species	δ [ppm] (^{19}F)	δ [ppm](^{31}P)	δ [ppm](^{1}H)
HF	-187.05 (s)	-	-
BF_4^-	-151.11, -151.16 (s)	-	-
$OPF(OH)_2$	-75.31 (d, ^1J = 931 Hz)	-10.09 (d, ^1J = 931 Hz)	-
OPF_2OH	-82.97 (d, ^1J = 961 Hz)	-20.63 (t, ^1J = 961 Hz)	-
OPF_2OCH_3	-84.31 (d, ^1J = 1005 Hz)	-21.37 (t, ^1J = 1005 Hz)	4.22 (d, ^4J = 12 Hz)
OPF_2OR	-86.19 (d, ^1J = 1005 Hz)	-20.31 (t, ^1J = 1005 Hz)	-
CH_3OH	-	-	3.35 (s)
H_2O	-	-	4.47 (s)

Table S5: Experimental ($\delta^{\mathrm{Exp.}}$) and DFT-calculated (δ^{DFT}) ^{1}H chemical shifts of comparable protons of $\mathbf{T_c}$ and $\mathbf{T_e}$. Both $\delta^{\mathrm{Exp.}}$ and δ^{DFT} are referenced against ^{1}H $\delta^{\mathrm{Exp.}}$ and ^{1}H δ^{DFT} respectively of tetramethylsilane at 0 ppm. δ^{DFT} of protons from methyl groups are averaged.

Atomic index	$\delta^{\mathrm{Exp.}}(\mathbf{T_c})$	$\delta^{\mathrm{Exp.}}(\mathbf{T_e})$	$\delta^{\mathrm{DFT}}(\mathbf{T_c})$	$\delta^{\mathrm{DFT}}(\mathbf{T_e})$	$\delta^{\mathrm{Exp.}}_{\mathbf{T_c}} - \delta^{\mathrm{Exp.}}_{\mathbf{T_e}}$	$\delta^{\mathrm{DFT}}_{\mathbf{T_c}} - \delta^{\mathrm{DFT}}_{\mathbf{T_e}}$
H-8,9,10,11	1.88, 1.94	1.67	1.82	1.61	0.21, 0.27	0.21
H-17	2.00	1.93	2.02	1.98	0.07	0.04
H-18,20	3.20	2.49	3.93	3.26	0.71	0.67
H-19,21	2.97	2.19	2.72	2.16	0.78	0.56
H-22	5.76	5.68	6.35	6.28	0.08	0.07
H-23	6.22	6.12	6.71	6.60	0.09	0.11
H-24	5.97	5.36	5.74	4.75	0.61	0.99

4.5 Stability of TMA in DMC containing 1 M LiTFSI

Figure S13 compares the ^{1}H NMR spectrum of TMA in DMC-d6 containing 1 M of LiTFSI (green) and $LiPF_6$ (black). After a week (t = 168 hours), signals broadened and shifted by paramagnetic relaxation (for instance, intrinsic CH_3 groups of TMA) are observed in case of LiTFSI, indicating the presence of a stable radical species, while resolved peaks from disproportionation products of TMA are observed in case of $LiPF_6$, indicating complete radical degradation.

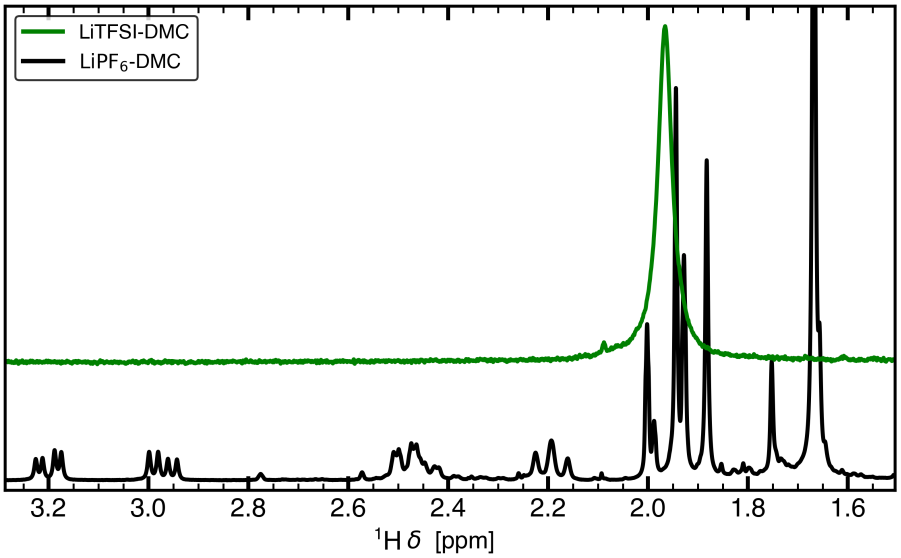

Figure S13: Comaprison of ^{1}H NMR spectrum of 20 mM TEMPO methacrylate in 1M LiTFSI in DMC-d6 (green) and 1M $LiPF_6$ in DMC-d6 (black) at t = 168 hours. The spectrum coloured green is vertically shifted for clarity.

4.6 NMR spectra of 1 after a week

^{1}H and ^{13}C–DEPT 135 NMR spectrum of **1** after complete radical degradation in DMC-d6 containing containing 1 M $LiPF_6$ is shown in Figure S14. The sample was kept in a sealed NMR tube for a week (t = 168 hours) before measurement. In contrast to NMR spectrum of **1** at t = 48 hours (see Figure S8(a)-(e)), the peaks corresponding to N-H and O-H groups become broad and the doublet splitting is no longer resolved after a week (t = 168 hours). Presence of HF is indicated by the broad peak at 10.40 ppm.[14] Other resonance peaks of $\mathbf{T}_e$ and $\mathbf{T}_c$ remain at the same chemical shift and exhibit the same J couplings as observed in the NMR spectrum of **1** at t = 48 hours. The total number of protons in the methyl region of the ^{1}H NMR spectrum was $\approx$ 30.

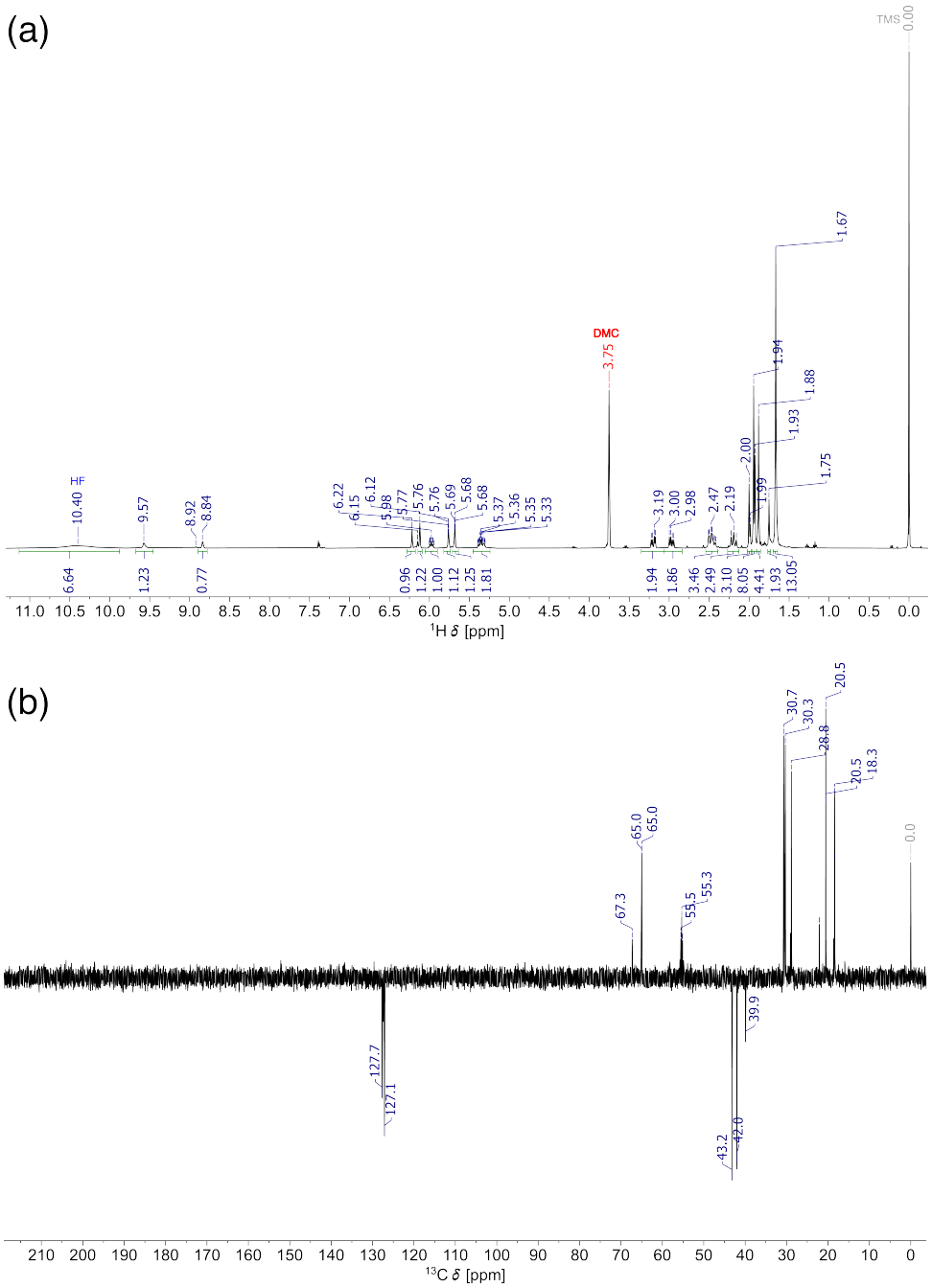

Figure S14: (a)^{1}H and (b)^{13}C–DEPT 135 NMR spectrum of **1** after a week (t=168 hours). Sample : 20 mM TMA in DMC-d6 containing 1 M $LiPF_6$

5 Laplace inversion

Laplace inversion of T_1 relaxation data for sample **1** and **2** was done without non-negativity constraint using an exponential kernel. Pre-processing of data and inversion parameters are described elsewhere.[16] The inversion was performed using home-written scripts that were run on Octave v. 6.4. The residuals from the fit of the T_1 time traces is shown in Figure S15 which were representative of random noise devoid of any systematic features and indicative of the compatibility of the chosen kernel. The T_1

relaxation distribution and two-Gaussian model fit for **1** is shown in Figure S16.

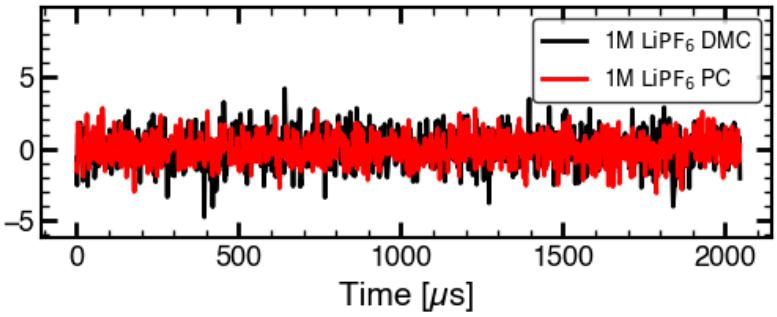

Figure S15: Residuals from ILT fits of T_1 data using an exponential kernel and without non-negativity constraint for samples **1** (black) and **2** (red).

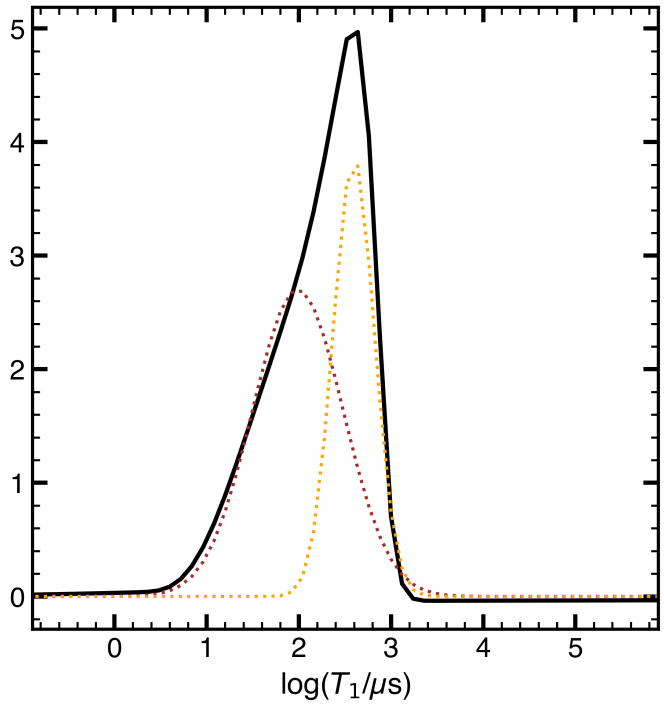

Figure S16: T_1 relaxation distribution of **1** obtained using Laplace inversion. Fast relaxing ($\approx$ 97 µs) and slow relaxing ($\approx$ 395 µs) components are denoted by brown and orange dotted lines respectively.

References

[1] S. Grimme, J. Antony, S. Ehrlich, H. Krieg, *The Journal of chemical physics* **2010**, *132*.

[2] S. Van Doorslaer, D. Goldfarb, S. Stoll, *EPR Spectroscopy: Fundamentals and Methods, Wiley* **2018**, pages 377–400.

[3] L. F. Ibáñez, J. Soetbeer, D. Klose, M. Tinzl, D. Hilvert, G. Jeschke, *Journal of Magnetic Resonance* **2019**, *307*, 106576.

[4] M. Shakourian-Fard, G. Kamath, S. K. Sankaranarayanan, *ChemPhysChem* **2016**, *17*, 2916.

[5] S. Stoll, A. Schweiger, *Journal of magnetic resonance* **2006**, *178*, 42.

[6] T.-L. Hwang, A. Shaka, *Journal of Magnetic Resonance, Series A* **1995**, *112*, 275.

[7] A. L. Davis, E. D. Laue, J. Keeler, D. Moskau, J. Lohman, *Journal of Magnetic Resonance (1969)* **1991**, *94*, 637.

[8] M. J. Thrippleton, J. Keeler, *Angewandte Chemie International Edition* **2003**, *42*, 3938.

[9] B. S. Parimalam, A. D. MacIntosh, R. Kadam, B. L. Lucht, *The Journal of Physical Chemistry C* **2017**, *121*, 22733.

[10] J. J. Helmus, C. P. Jaroniec, *Journal of biomolecular NMR* **2013**, *55*, 355.

[11] S. Wilken, M. Treskow, J. Scheers, P. Johansson, P. Jacobsson, *Rsc Advances* **2013**, *3*, 16359.

[12] G. Ceccarelli, F. Andruzzi, *Die Makromolekulare Chemie: Macromolecular Chemistry and Physics* **1979**, *180*, 1371.

[13] S. Wiemers-Meyer, M. Winter, S. Nowak, *Physical Chemistry Chemical Physics* **2016**, *18*, 26595.

[14] B. L. Rinkel, J. P. Vivek, N. Garcia-Araez, C. P. Grey, *Energy & environmental science* **2022**, *15*, 3416.

[15] G. R. Fulmer, A. J. Miller, N. H. Sherden, H. E. Gottlieb, A. Nudelman, B. M. Stoltz, J. E. Bercaw, K. I. Goldberg, *Organometallics* **2010**, *29*, 2176.

[16] J. Granwehr, P. J. Roberts, *Journal of chemical theory and computation* **2012**, *8*, 3473.